Theor Chem Acc (2009) 124:279–294
DOI 10.1007/s00214-009-0609-x

REGULAR ARTICLE

How critical fluctuations influence adsorption properties of a van der Waals fluid onto a spherical colloidal particle

Shiqi Zhou

Received: 23 April 2009 / Accepted: 9 July 2009 / Published online: 29 July 2009

Abstract A recently proposed 3rd-order thermodynamic perturbation theory (TPT) is extended to its 5th-order version and non-uniform counterpart by supplementing with density functional theory (DFT) and a number of ansatzs for a bulk 2nd-order direct correlation function (DCF). Employment of the ansatzs DCF enables the resultant non-uniform formalism devoid of any adjustable parameter and free from numerically solving an Ornstein–Zernike integral equation theory. Density profiles calculated by the present non-uniform formalism for a hard core attractive Yukawa (HCAY) fluid near a spherical geometry are favorably compared with corresponding simulation data available in literature, and are more accurate than those based on a previous 3rd + 2nd-order perturbation DFT. The non-uniform 5th-order TPT is employed to investigate adsorption of the HCAY fluid onto a colloidal particle; it is disclosed that a depletion adsorption can be induced when the coexistence bulk fluid is situated in neighborhood of a critical point or near a bulk vapor–liquid coexistence gaseous phase or liquid phase density. A physical interpretation is given for such depletion adsorption and for its connection with parameters of the potential under consideration, which is ascribed to critical density fluctuations existing within a wide region of the bulk diagram. For a large spherical external potential inducing wetting transition, it is found that only round wetting transition is found instead of 1st-order pre-wetting transition in the case of a planar wall external potential, and the wetting transition temperature increases relative to that for the planar wall external potential. The present theoretical results for wetting transitions are supported by previous investigation based on thermodynamic considerations and a phenomenological Landau mean field theory, and are also in conformity with the present qualitative physical interpretation.

Keywords Adsorption · Interface · Yukawa potential · Colloids

S. Zhou
State Key Laboratory of Powder Metallurgy,
Central South University, 410083 Changsha, Hunan, China

S. Zhou (✉)
School of Physics Science and Technology,
Central South University, 410083 Changsha, Hunan, China
e-mail: chixiayzsq@yahoo.com

1 Introduction

For a long time, thermodynamic perturbation theory (TPT) plays key roles as fast computational tools in many fields, such as thermodynamic properties of bulk phases [1] including gas phase, liquid phase and solid phase [2], structure and thermodynamic properties of inhomogeneous phases [3] such as density distribution profiles and phase transitions under confined conditions, and solvation free energy [4, 5], etc. Recently the present author proposes a high order version of the TPT, a 3rd-order TPT [6–8]; it is indicated that the 3rd-order TPT constitutes a significant improvement over a traditional 1st-order TPT [9] and 2nd-order macroscopic compressibility approximation (MCA) [10, 11]—TPT for calculation of the bulk thermodynamic properties of many model fluids. In the framework of classical density functional theory (DFT), the simplest equation of state, i.e., van der Waals mean field theory, can be extended to its non-uniform counterpart. In fact, the 2nd-order MCA-TPT has also been extended to its non-uniform version. Unfortunately, the non-uniform versions of these low order TPTs suffer from grave accuracy problem which enables these non-uniform versions only qualitative. Considering that the new 3rd-order TPT is

highly accurate and quantitatively satisfactory even when the 2nd-order MCA-TPT qualitatively fails [8], it is of practical significance to extend the new 3rd-order or its higher order version to non-uniform situation in the framework of the classical DFT, the resultant non-uniform version will be expected to be of higher accuracy.

The present paper is arranged as follows. In Sect. 2 we devise a theoretical way by which the TPT of any order can be extended to its non-uniform counterpart. By extending the 3rd-order TPT to 5th-order version which then is combined with the theoretical way, we acquire a non-uniform 5th-order TPT which is then employed to calculate density profiles of a sample hard core attractive Yukawa (HCAY) fluid subjected to a spherical geometry and tested by a comparison of the resultant density profiles with those based on an existing 3rd + 2nd-order perturbation DFT [12, 13] and computer simulation [13]. In Sect. 3, the present non-uniform 5th-order TPT is employed to investigate adsorption behavior of the HCAY fluid onto a spherical colloidal particle under condition that the coexistence bulk fluid is situated in a neighborhood of the critical point or near a gaseous phase or liquid phase side of the bulk vapor–liquid coexistence curve. Finally we summarize the present paper by drawing some concluding remarks in Sect. 4.

2 Methods

In a coupling parameter expansion underlying the 3rd-order TPT [6–8], the uniform excess Helmholtz free energy $F_{\mathrm{ex}}(\rho_{\mathrm{b}})$ for a system of N particles in a volume V at temperature T interacting via a full pair potential $u(r)$ is given by

$$F_{\mathrm{ex}}(\rho_{\mathrm{b}}) = F_{\mathrm{ex\text{-}ref}}(\rho_{\mathrm{b}}) + \sum_{n=1}^{\infty} \frac{1}{n!} N 2\pi\rho_{\mathrm{b}} \times \int dr r^2 u_{\mathrm{per}}(r) \left. \frac{\partial^{(n-1)} g(r,\xi,\rho_{\mathrm{b}},T)}{\partial \xi^{(n-1)}} \right|_{\xi=0} . \quad (1)$$

Here, $F_{\mathrm{ex\text{-}ref}}(\rho_{\mathrm{b}})$ is the excess Helmholtz free energy of a reference fluid with a pair potential u_{ref} and bulk density ρ_{b}, $u_{\mathrm{per}}(r)$ is the perturbation part of the whole potential $u(r)$ given by

$$u(r) = u_{\mathrm{ref}}(r) + u_{\mathrm{per}}(r). \quad (2)$$

At the present stage of the 3rd-order TPT [6–8], $u_{\mathrm{ref}}(r)$ is a hard sphere potential given by

$$u_{\mathrm{ref}} = \begin{array}{ll} \infty & r<\sigma \\ 0 & r<\sigma \end{array} \quad (3)$$

$g(r, \xi, \rho_{\mathrm{b}}, T)$ is a radial distribution function (rdf) of a bulk fluid with a pair potential $u(r; \xi)$ given by

$$u(r;\xi) = u_{\mathrm{ref}}(r) + \xi u_{\mathrm{per}}(r). \quad (4)$$

$\left. \frac{\partial^{(n-1)} g(r,\xi,\rho_{\mathrm{b}},T)}{\partial \xi^{(n-1)}} \right|_{\xi=0}$ is the $(n-1)$th order derivative evaluated at $\xi = 0$ of $g(r, \xi, \rho_{\mathrm{b}}, T)$ with respect to ξ, $\left. \frac{\partial^0 g(r,\xi,\rho_{\mathrm{b}},T)}{\partial \xi^0} \right|_{\xi=0} = g(r, 0, \rho_{\mathrm{b}}, T)$ is the rdf of the hard sphere fluid of density ρ_{b} and diameter σ.

In Refs. [6–8], the perturbation expansion series is truncated at $n = 3$. In fact, the higher version is also possible, but the numerical implementation needs more caution. As in Refs. [6–8], the higher order terms are concerned with calculation of derivatives of the $g(r, \xi, \rho_{\mathrm{b}}, T)$ w.r.t. ξ at $\xi = 0$. Following Refs. [6–8], one calculates $g(r, \xi, \rho_{\mathrm{b}}, T)$ with $\xi = 0, \pm\Delta\xi, \pm 2\Delta\xi, \pm 3\xi, \pm 4\xi$, then $\left. \frac{\partial^{(n-1)} g(r,\xi,\rho_{\mathrm{b}},T)}{\partial \xi^{(n-1)}} \right|_{\xi=0}$ for $n \leq 5$ can be obtained by finite difference technique. As for the numerical solution of the OZ integral equation theory for $g(r, \xi, \rho_{\mathrm{b}}, T)$, one can refer to Refs. [6–8]. It should be pointed out that in Refs. [6–8] only $g(r, \xi, \rho_{\mathrm{b}}, T)$ with $\xi = 0, \pm\Delta\xi, \pm 2\Delta\xi$ needs to be calculated to obtain $\left. \frac{\partial^{(n-1)} g(r,\xi,\rho_{\mathrm{b}},T)}{\partial \xi^{(n-1)}} \right|_{\xi=0}$ for $n \leq 3$. At present time, we cannot obtain $\left. \frac{\partial^{(n-1)} g(r,\xi,\rho_{\mathrm{b}},T)}{\partial \xi^{(n-1)}} \right|_{\xi=0}$ for $n > 5$ because of accumulating errors due to the finite difference technique.

The resultant 5th-order TPT will be employed throughout the present paper for construction of a non-uniform version of the TPT, but any variant of the TPT can be inserted into the present non-uniform formalism, the only difference is that the resultant non-uniform formalism will show some change in the prediction accuracy due to the different accuracy of the employed TPTs.

Hence, the employed 5th-order TPT is given by:

$$F_{\mathrm{ex}}(\rho_{\mathrm{b}}) = F_{\mathrm{ex\text{-}ref}}(\rho_{\mathrm{b}}) + \sum_{n=1}^{5} \frac{1}{n!} N 2\pi\rho_{\mathrm{b}} \times \int dr r^2 u_{\mathrm{per}}(r) \left. \frac{\partial^{(n-1)} g(r,\xi,\rho_{\mathrm{b}})}{\partial \xi^{(n-1)}} \right|_{\xi=0} \quad (5)$$

where $F_{\mathrm{ex\text{-}ref}}(\rho_{\mathrm{b}})$ is given by a Carnahan–Starling (CS) equation of state for the hard sphere fluid [14].

It should be pointed out that by following to Eq. 6 of Ref. 6, one can obtain $F_{\mathrm{ex}}(\rho_{\mathrm{b}})$ by integrating $g(r, \xi, \rho_{\mathrm{b}}, T)$ over ξ from 0 to 1, i.e., $F_{\mathrm{ex}}(\rho_{\mathrm{b}}) = F_{\mathrm{ex-ref}}(\rho_{\mathrm{b}}) + N2\pi\rho_{\mathrm{b}} \int dr r^2 u_{\mathrm{per}}(r) \int_0^1 d\xi g(r, \xi, \rho_b, T)$. Out of two considerations we have not calculated $g(r, \xi, \rho_{\mathrm{b}}, T)$ for ξ ranging from 0 to 1 and calculated the dual integrals. First, one cannot expect to obtain accurate $g(r, \xi, \rho_{\mathrm{b}}, T)$ for values of ξ deviating obviously from 0; then with an inaccurate $g(r, \xi, \rho_{\mathrm{b}}, T)$ for values of ξ not close to zero, the results from the dual integrals will not be more accurate than those from the scheme adopted in the present perturbation approach. In fact, if one knows the accurate

$g(r, 1, \rho_b, T)$, one will not bother to calculate the dual integral which is concerned with information of $g(r, \xi, \rho_b, T)$ for $0 \leq \xi \leq 1$. One will prefer to obtain the virial pressure first, then integrate the virial pressure to obtain $F_{ex}(\rho_b)$. Second, when the temperatures of interest is below the critical temperature, the OZ integral equation will lose physical solution when $\xi = 1$; the larger the value of ξ, the higher the starting temperature for which the OZ integral equation will lose physical solution. The above situation makes the resultant theory employing the dual integrals break down when the temperature of interest drops below the critical temperature and the density of interest enter into the vapor–liquid coexistence region of the phase diagram.

In the classical DFT, the equilibrium density profile $\rho(\mathbf{r})$ is calculated by an Euler–Lagrange equation for a grand canonical potential,

$$\rho(\mathbf{r}) = \rho_b \exp\left\{-\beta\varphi_{ext}(\mathbf{r}) + C^{(1)}(\mathbf{r}; [\rho]) - C_0^{(1)}(\rho_b)\right\} \quad (6)$$

where $C^{(1)}(\mathbf{r}; [\rho])$ is the 1st-order DCF of the non-uniform fluid, $C_0^{(1)}(\rho_b)$ is the uniform 1st-order DCF of the corresponding coexistence bulk fluid with density ρ_b.

$C^{(1)}(\mathbf{r}; [\rho])$ is mathematically the 1st-order functional derivative of the excess Helmholtz free energy density functional $F_{ex}[\rho(\mathbf{r})]$ w.r.t $\rho(\mathbf{r})$:

$$C^{(1)}(\mathbf{r}; [\rho]) = \frac{-\delta\beta F_{ex}[\rho]}{\delta\rho(\mathbf{r})}. \quad (7)$$

It has been a long practice to divide the underlying potential into a short-ranged repulsion part and a long-ranged tail part, then attack the two resultant parts by different routes. In recently published literatures, it has been generally accepted [15] that a weighted density approximation (WDA) should substitute a local density approximation for the treatment of the short-ranged repulsion part. The WDA consists in substituting the density argument of the bulk excess Helmholtz free energy by a weighted density to formulate the non-uniform excess Helmholtz free energy, calculation of the weighted density incurs an integration of the practical density profile weighted by a weighting function w. The WDA goes through several stages of development. The earliest version of the WDA is perhaps that of Nordholm et al. [16, 17] with a weighting function proportional to the Heaviside step function. Tarazona [18] and Curtin and Ashcroft [19] propose specifying the weighting function by enforcing the uniform limit of the second functional derivative of the excess Helmholtz free energy functional w.r.t. the density profile equal to the bulk 2nd-order DCF. The weighted density and weighting function are coupled together whether it is based on the Tarazona's recipe or the Curtin–Ashcroft's recipe. Rosenfeld proposes a variant [20] of the WDA, fundamental measure functional for the non-uniform single and binary hard sphere mixture; in this recipe the weighted density and weighting function are decoupled. The present author proposes a simple weighted density approximation (SWDA) [21] in which the weighted density and weighting function are also decoupled. Although a crude approximation, the SWDA surely finds widespread applications in the DFT practices [22–25]. Especially the SWDA supplies an appropriate weighted density for use in recent density functional approximations [26]. In fact, the undesirable inaccuracy originating from the naive decoupling approximation underlying the SWDA can be weakened and digested by a so-called Lagrangian theorem-based density functional approximation (LTDFA) [27]. As for the long-ranged tail part, several different methods are adopted which fall into three categories, they are mean field approximation [28], hard sphere weighted density perturbation approximation [29], and tail weighted density approximation (TWDPA) [30–32]. We will employ the TWDPA, but the involved weighted density is based on the SWDA [21] due to its simplicity.

We will follow the usual procedure to partition the potential into short-ranged repulsion part and long-range tail part. Correspondingly, the structure and thermodynamic quantities are also divided into the short-ranged repulsion part and long-range tail part:

$$F_{ex}[\rho(\mathbf{r})] = F_{ex\text{-}hc}[\rho(\mathbf{r})] + F_{ex\text{-}tail}[\rho(\mathbf{r})], \quad (8)$$

$$C^{(1)}(\mathbf{r}; [\rho]) = C_{hc}^{(1)}(\mathbf{r}; [\rho]) + C_{tail}^{(1)}(\mathbf{r}; [\rho]), \quad (9)$$

$$F_{ex}(\rho_b) = F_{ex\text{-}hc}(\rho_b) + F_{ex\text{-}tail}(\rho_b), \quad (10)$$

$$C_0^{(1)}(\rho_b) = C_{0-hc}^{(1)}(\rho_b) + C_{0-tail}^{(1)}(\rho_b). \quad (11)$$

Correspondingly, one has:

$$C^{(1)}(\mathbf{r}; [\rho]) - C_0^{(1)}(\rho_b) = \left[C_{hc}^{(1)}(\mathbf{r}; [\rho]) - C_{0-hc}^{(1)}(\rho_b)\right] + \left[C_{tail}^{(1)}(\mathbf{r}; [\rho]) - C_{0-tail}^{(1)}(\rho_b)\right]. \quad (12)$$

Considering that the 5th-order TPT uses the hard sphere fluid as the reference system, concomitantly we should assume $F_{ex\text{-}hc}(\rho_b) = F_{ex\text{-}ref}(\rho_b)$. As for the treatment of $F_{ex-hc}[\rho(\mathbf{r})]$, we will employ the LTDFA [27] which gives:

$$C_{hc}^{(1)}(\mathbf{r}; [\rho]) - C_{0-hc}^{(1)}(\rho_b) = \int d\mathbf{r}_1 (\rho(\mathbf{r}_1) - \rho_b) \times C_{0-hs-PY}^{(2)}(|\mathbf{r} - \mathbf{r}_1|; \tilde{\rho}_{hc}((\mathbf{r} + \mathbf{r}_1)/2, \lambda)), \quad (13)$$

where the hard core weighted density $\tilde{\rho}_{hc}$ is given by

$$\tilde{\rho}_{hc}((\mathbf{r} + \mathbf{r}_1)/2, \lambda) = \int d\mathbf{r}' C_{0-hs-PY}^{(2)}(|(\mathbf{r} + \mathbf{r}_1)/2 - \mathbf{r}'|; \rho_b) \times [\rho_b + \lambda(\rho(\mathbf{r}') - \rho_b)] \Big/ C_{0-hs-PY}^{(1)\prime}(\rho_b) \quad (14)$$

In the Eqs. 13 and 14, $C^{(n)}_{0-\mathrm{hs-PY}}$ stands for a bulk hard sphere fluid nth-order DCF, $C^{(1)}_{0-\mathrm{hs-PY}}{}'(\rho_\mathrm{b})$ stands for the 1st-order derivative of the bulk hard sphere fluid 1st-order DCF w.r.t. the density argument ρ_b. The subscript PY means that $C^{(n)}_{0-\mathrm{hs-PY}}$ and $C^{(1)}_{0-\mathrm{hs-PY}}{}'(\rho_\mathrm{b})$ are obtained under Percus–Yevick approximation [33, 34] for the OZ integral equation theory. Throughout the text, the subscript 0 means that the quantity is for the bulk case, absence of the subscript 0 corresponds to non-uniform situation. Regarding the numerical value of the parameter λ, we will discuss it later in the text.

As for $C^{(1)}_{\mathrm{tail}}(\mathbf{r};[\rho])$, we employ the WDA which gives:

$$F_{\text{ex-tail}}[\rho(\mathbf{r})] = \int d\mathbf{r}\rho(\mathbf{r})f_{\text{ex-tail}}(\tilde{\rho}_{\mathrm{tail}}(\mathbf{r})), \tag{15}$$

where $f_{\text{ex-tail}}$ is a bulk excess Helmholtz free energy per particle for the tail part only. Considering that we have assumed $F_{\text{ex-hc}}(\rho_\mathrm{b}) = F_{\text{ex-ref}}(\rho_\mathrm{b})$, therefore we have,

$$f_{\text{ex-tail}}(\rho_\mathrm{b}) = F_{\text{ex-tail}}(\rho_\mathrm{b})/N = (F_{\text{ex}}(\rho_\mathrm{b}) - F_{\text{ex-ref}}(\rho_\mathrm{b}))/N \tag{16}$$

the weighted density $\tilde{\rho}_{\mathrm{tail}}(\mathbf{r})$ is calculated by the SWDA [21],

$$\tilde{\rho}_{\mathrm{tail}}(\mathbf{r}) = \int d\mathbf{r}'\rho(\mathbf{r}')w(|\mathbf{r}-\mathbf{r}'|;\rho_\mathrm{b}), \tag{17}$$

$$w(r;\rho_\mathrm{b}) = C^{(2)}_{0-\mathrm{tail}}(r;\rho_\mathrm{b}) \Big/ \int d\mathbf{r}C^{(2)}_{0-\mathrm{tail}}(r;\rho_\mathrm{b}), \tag{18}$$

$C^{(2)}_{0-\mathrm{tail}}(r;\rho_\mathrm{b})$ is a tail part of the bulk 2nd-order DCF $C^{(2)}_0(r;\rho_b)$ of the full pair potential $u(r)$. In parallel with Eq. 7, one has,

$$\begin{aligned} C^{(1)}_{\mathrm{tail}}(\mathbf{r};[\rho]) &= \frac{-\delta\beta F_{\text{ex-tail}}[\rho]}{\delta\rho(\mathbf{r})} \\ &= -\beta f_{\text{ex-tail}}(\tilde{\rho}_{\mathrm{tail}}(\mathbf{r})) \\ &\quad - \int d\mathbf{r}'\rho(\mathbf{r}')\beta f'_{\text{ex-tail}}(\tilde{\rho}_{\mathrm{tail}}(\mathbf{r}'))w(|\mathbf{r}-\mathbf{r}'|;\rho_\mathrm{b}), \end{aligned} \tag{19}$$

imposing limit of $\rho(\mathbf{r}) \to \rho_\mathrm{b}$ on $C^{(1)}_{\mathrm{tail}}(\mathbf{r};[\rho])$, one obtains $C^{(1)}_{0-\mathrm{tail}}(\rho_\mathrm{b})$

$$\begin{aligned} C^{(1)}_{0-\mathrm{tail}}(\rho_\mathrm{b}) &= \lim_{\rho(\mathbf{r})\to\rho_\mathrm{b}} C^{(1)}_{\mathrm{tail}}(\mathbf{r};[\rho]) \\ &= -\beta f_{\text{ex-tail}}(\rho_\mathrm{b}) - \beta\rho_\mathrm{b} f'_{\text{ex-tail}}(\rho_\mathrm{b}). \end{aligned} \tag{20}$$

Substituting Eqs. 12, 13, 19, and 20 into Eq. 6, one obtains

$$\begin{aligned} \rho(\mathbf{r}) = \rho_\mathrm{b}\exp\{&-\beta\varphi_{\text{ext}}(\mathbf{r}) + \int d\mathbf{r}_1(\rho(\mathbf{r}_1)-\rho_\mathrm{b}) \\ &\times C^{(2)}_0(|\mathbf{r}-\mathbf{r}_1|;\tilde{\rho}_{\mathrm{hc}}((\mathbf{r}+\mathbf{r}_1)/2,\lambda)) \\ &- \beta f_{\text{ex-tail}}(\tilde{\rho}_{\mathrm{tail}}(\mathbf{r})) \\ &- \int d\mathbf{r}'\rho(\mathbf{r}')\beta f'_{\text{ex-tail}}(\tilde{\rho}_{\mathrm{tail}}(\mathbf{r}'))w(|\mathbf{r}-\mathbf{r}'|;\rho_\mathrm{b}) \\ &+ \beta f_{\text{ex-tail}}(\rho_\mathrm{b}) + \beta\rho_\mathrm{b} f'_{\text{ex-tail}}(\rho_\mathrm{b})\}. \end{aligned} \tag{21}$$

In Eq. 21, $\tilde{\rho}_{\mathrm{hc}}$ and $\tilde{\rho}_{\mathrm{tail}}$ are calculated respectively by Eqs. 14 and 17.

Now the only undetermined quantity is $C^{(2)}_{0-\mathrm{tail}}(r;\rho_\mathrm{b})$. Considering that one has employed $C^{(2)}_{0-\mathrm{hs-PY}}$ for the treatment of the hard core part, one should remove away $C^{(2)}_{0-\mathrm{hs-PY}}$ from $C^{(2)}_0(r;\rho_\mathrm{b})$ to obtain $C^{(2)}_{0-\mathrm{tail}}(r;\rho_\mathrm{b})$. Therefore, a key quantity is $C^{(2)}_0(r;\rho_\mathrm{b})$, whose analytical expression will be given in the present paper.

We propose several ansatzs for the construction of $C^{(2)}_0(r;\rho_\mathrm{b})$. One is that $C^{(2)}_{0-\mathrm{tail}}(r;\rho_\mathrm{b})$ should conform with a zero density limit (ZDL) denoted by Eq. 22

$$C^{(2)}_{0-\mathrm{tail}}(r;\rho_\mathrm{b}) = \exp(-\beta u(r)) - 1 \quad r \geq \sigma, \tag{22}$$

the other is that the core part of $C^{(2)}_0(r;\rho_\mathrm{b})$ with $r \leq \sigma$ should be similar to $C^{(2)}_{0-\mathrm{hs-PY}}(r;\rho_\mathrm{b})$ since both of them describe the hard core repulsion. But they should not be equal since $C^{(2)}_0(r;\rho_\mathrm{b})$ with $r \leq \sigma$ is influenced by the long-range tail. Following these considerations, we propose following approximation,

$$C^{(2)}_0(r;\rho_\mathrm{b}) = \chi C^{(2)}_{0-\mathrm{hs-PY}}(r;\rho_\mathrm{b}) \quad r < \sigma. \tag{23}$$

Combining Eqs. 22 and 23 one obtains,

$$\begin{aligned} C^{(2)}_0(r;\rho_\mathrm{b}) = \chi C^{(2)}_{0-\mathrm{hs-PY}}(r;\rho_\mathrm{b}) \quad & r < \sigma \\ \exp(-\beta u(r)) - 1 \quad & r \geq \sigma \end{aligned} \tag{24}$$

As for the specification of the parameter χ, we will determine it by thermodynamic self-consistency condition given by

$$1 - \rho_\mathrm{b}\int d\mathbf{r}C^{(2)}_0(r;\rho_\mathrm{b}) = 1/\chi_\mathrm{T} = (\partial\beta P/\partial\rho_\mathrm{b})_\mathrm{T} \tag{25}$$

Equation 25 means a self-consistency between the excess Helmholtz free energy and the correlation function for each density. $(\partial\beta P/\partial\rho_\mathrm{b})_T$ will be calculated by the uniform 5th-order TPT.

$C^{(2)}_{0-\mathrm{tail}}(r;\rho_\mathrm{b})$ is thus obtained by disposing $C^{(2)}_{0-\mathrm{hs-PY}}(r;\rho_\mathrm{b})$ from $C^{(2)}_0(r;\rho_\mathrm{b})$:

$$\begin{aligned} C^{(2)}_{0-\mathrm{tail}}(r;\rho_\mathrm{b}) = (\chi-1)C^{(2)}_{0-\mathrm{hs-PY}}(r;\rho_\mathrm{b}) \quad & r < \sigma \\ \exp(-\beta u(r)) - 1 \quad & r \geq \sigma \end{aligned} \tag{26}$$

Equation 26 makes use of the fact that $C^{(2)}_{0-\mathrm{hs-PY}}(r;\rho_\mathrm{b})$ disappears for $r > \sigma$.

Finally, we recall that for the inter-particle potential with an attractive tail $C^{(2)}_{0-\mathrm{tail}}(r;\rho_\mathrm{b})$ is usually positively valued. Hence, one should substitute χ by χ_p given by

$$\begin{aligned} \chi_\mathrm{p} = \chi \quad & \chi \leq 1 \\ 1 \quad & \chi > 1 \end{aligned} \tag{27}$$

To conclude, the final expression for our bulk 2nd-order DCF is given by

$$C^{(2)}_{0-\mathrm{tail}}(r;\rho_b) = \begin{cases} (\chi_p - 1)C^{(2)}_{0-\mathrm{hs-PY}}(r;\rho_b) & r<\sigma \\ \exp(-\beta u(r)) - 1 & r \geq \sigma. \end{cases} \quad (28)$$

It should be pointed out that the introduction of the parameter χ_p destroys the complete self-consistency between the excess Helmholtz free energy and the correlation function when χ becomes larger than 1. Considering that the bulk 2nd-order DCF denoted by Eq. 24 is itself approximate, complete thermodynamic self-consistency cannot certainly ensure more accurate approximation than partial thermodynamic self-consistency (PTS), therefore we will still employ the Eq. 28. With the Eq. 28 employed for calculation of $w(r;\rho_b)$ by Eq. 18, the resultant non-uniform TPT is denoted as non-uniform 5th-order TPT-ZDL-PTS.

When one fixes the physical parameter λ at 0.5, as done in the adjustable parameter free version [35] of the LTDFA [27], the resultant predictions for the density profiles of the HCAY fluid as simulated in Ref. [13] deviate sometimes obviously from the corresponding simulation results, the contact densities for the hard geometries are generally lower than those of the simulation situation. Therefore, one has to adjust the value of the parameter λ to be below 0.5, as done in the original LTDFA [27] in which the parameter λ is specified by a hard wall sum rule [36]. Extensive sample calculations indicate that a constant parameter $\lambda = 0.45$ is sufficient for the present non-uniform 5th-order TPT-ZDL-PTS to achieve the most satisfactory performance on average for all of the situations simulated in Ref. [13]. This is very fortunate as one does not bother to determine the parameter λ beforehand for each coexistence bulk state. The 'good fortune' is not an accidental phenomena as similar 'good fortune' also appears in a recently proposed polymer melt DFT approach [37] in which the parameter λ can be fixed at 0.5 as exactly required by the adjustable parameter free version [35] of the LTDFA [27]. A common point for both the present situation and that in Ref. [37] is that the bulk 2nd-order DCFs employed in these two approaches are scaled by the respective equation of state. Therefore, the scaling of the bulk 2nd-order DCF should be a necessary condition for the holding of the adjustable parameter free version [35] of the LTDFA [27]. As for the small deviation of the present $\lambda = 0.45$ from the exact $\lambda = 0.5$, this can be ascribed to: (1) the systematical errors originating from the ansatzs bulk 2nd-order DCF which are obtained from several assumptions or boundary conditions on the DCF, instead of solving the OZ integral equation accurately, (2) the fact that λ value specified by the hard wall sum rule in the original LTDFA [27] is itself smaller than 0.5.

We will test the accuracy of the non-uniform 5th-order TPT-ZDL-PTS for calculation of the density profiles of the HCAY fluid subjected to various types of external potential and maintaining equilibrium with the bulk fluid, when the latter is in the state of (1) supercritical temperature but close to the critical value with the density ranging from low to high density region, and (2) subcritical temperature with the density near the vapor–liquid coexistence line.

We investigate several cases of the source for the external potential. Besides the usual single hard wall, we treat also a spherical cavity surrounded by a spherical hard wall, a planar gap, i.e., the two hard walls separated by a distance L, a large hard spherical particle, and a bulk HCAY particle.

The two sample external potentials, which will be mainly investigated in the present paper, are respectively due to the presence of the large hard spherical particle and the bulk HCAY particle, and respectively given by

$$\varphi_{\mathrm{ext}}(\mathbf{r}) = \begin{cases} \propto & |\mathbf{r}|<R \\ = 0 & |\mathbf{r}| > R \end{cases} \quad (29)$$

for a large hard spherical particle of radius R, and

$$\varphi_{\mathrm{ext}}(\mathbf{r}) = u_{\mathrm{HCAY}}(r) = -\varepsilon\sigma \exp[-\kappa^*(r-\sigma)/\sigma]/r \quad (30)$$

for a bulk HCAY particle situated at the origin. For the latter case, the reduced density distribution function $\rho(\mathbf{r})/\rho_b$ is actually the bulk RDF $g(\mathbf{r})$ according to the Percus's test particle method [38].

The present theoretical predictions for the density profiles of the HCAY fluid due to the external potentials given by Eqs. 29 and 30 are presented in Figs. 1, 2, 3, 4, 5, 6, 7 and 8 together with the corresponding simulation results available in literature [13]. The simulation results are represented by symbols to distinguish from the theoretical predictions denoted by lines. A detailed comparison of the present Figs. 1–8 with Figs. 8–15 in Ref. [13], where the theoretical predictions are based on a 3rd + 2nd-order perturbation DFT [12, 13], will be given. We have not presented the 3rd + 2nd-order perturbation DFT predictions in the present Figs. 1–8 only to make the figures clear enough since each one of the present Figs. 1–8 presents several curves corresponding to different coexistence bulk densities.

For the external field due to the bulk HCAY particle denoted by Eq. 30, the two theoretical approaches behave well for the calculation of the RDF $g(\mathbf{r})$. However, it is still easy to observe the higher accuracy (Figs. 1, 2, 3, 4) of the present approach over that of the 3rd + 2nd-order perturbation DFT [12, 13]. For the external field due to a large hard spherical particle denoted by Eq. 29, the two approaches are comparable in accuracy for a parameter combination of $k^* = 1.8$, $T^* = 1.25$ (Fig. 5). But for the parameter combinations of $k^* = 3.0$, $T^* = 0.76$ and $k^* = 4.0$, $T^* = 0.61$ (Figs. 6, 7), the non-uniform 5th-order TPT-ZDL-PTS performs better than the 3rd + 2nd-order perturbation DFT does. For all of the investigated

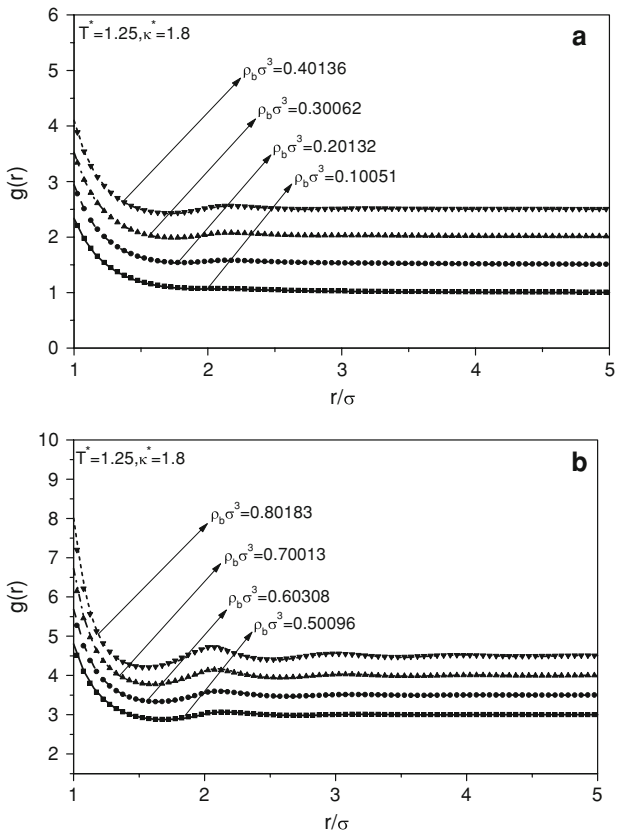

Fig. 1 **a** The theoretical (*lines*) and simulation (*symbols*) [13] results for the RDF of the HCAY model fluid at the bulk densities and potential parameters as shown. For the reason of clarity, the data corresponding to individual densities are shifted upwards by different factors (0.5, 1, 1.5, etc.). **b** Same as in **a** but for the bulk coexistence densities as shown

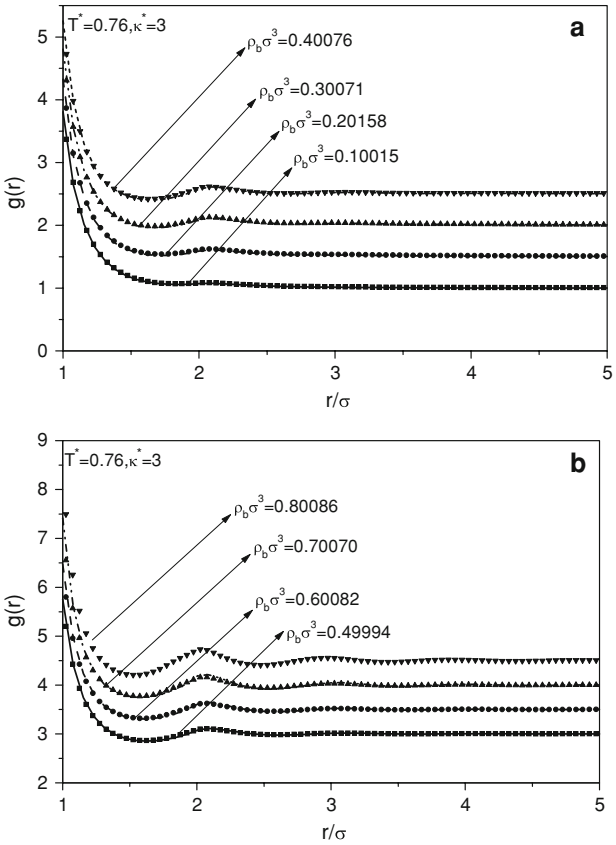

Fig. 2 **a** Same as in Fig. 1a but for the bulk parameters as shown. **b** Same as in **a** but for the bulk coexistence densities as shown

subcritical temperature cases (Fig. 8), the present approach is also superior to the 3rd + 2nd-order perturbation DFT.

As for the situations of other hard geometries such as the single hard wall, the spherical cavity, and the planar gap, the conclusion is also more favorable for the present non-uniform 5th-order TPT-ZDL-PTS than for the 3rd + 2nd-order perturbation DFT, we have not presented the calculated density profiles for these three hard geometries only out of a consideration of page limit.

It has been indicated [39] that the 3rd + 2nd-order perturbation DFT [12, 13] is physically reliable, it is the poor accuracy of the employed mean spherical approximation (MSA) in Ref. [13] that enables the satisfactory performance of the 3rd + 2nd-order perturbation DFT for a combination of single hard wall and long-ranged HCAY tail with $k^* = 1.8$ cannot go on for other external fields and other parameter combinations. This fact only brings out the superiority of the present ansatzs bulk 2nd-order DCF over the MSA for the OZ integral equation. Our ansatzs bulk 2nd-order DCF is free from solving numerically the OZ integral equation, therefore its application is not limited to several simple potentials for which analytical bulk 2nd-order DCFs are available in literature. Obviously the satisfactory performance of the present bulk 2nd-order DCF comes from the imposition of the PTS and the satisfactory accuracy of the present uniform 5th-order TPT as input. It should be pointed out that the sample coexistence bulk states are near the critical point or near the vapor–liquid coexistence lines, therefore the present test is harsh. Absence of any adjustable parameter from the present formalism enables the approach very convenient for theoretical investigation which needs intensive calculations as done in the next section.

3 Results and discussion

To systematically and quantitatively investigate the adsorption of the HCAY fluid onto a spherical colloid particle, in the first place we define a reduced excess adsorption Γ^*_{ex},

$$\Gamma^*_{ex} = \sigma^2 \int_R^\infty 4\pi r^2 [\rho(\mathbf{r}) - \rho_b] \mathrm{d}r \Big/ \left(4\pi R^2\right). \tag{31}$$

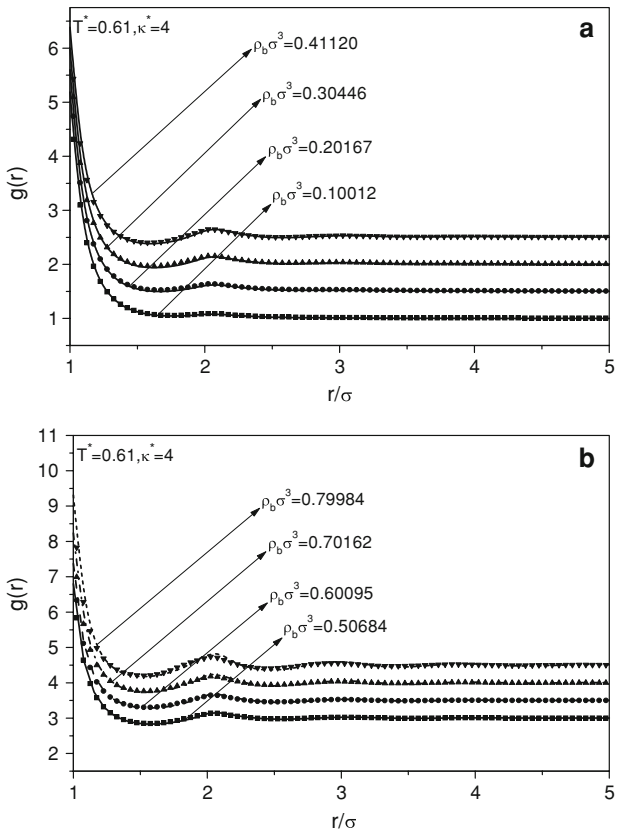

Fig. 3 **a** Same as in Fig. 1a but for the bulk parameters as shown. **b** Same as in **a** but for the bulk coexistence densities as shown

One sample external field is given by

$$\begin{aligned}\beta\varphi_{\text{ext}}(\mathbf{r}) &= \propto && |\mathbf{r}|<R \\ &= \beta\varepsilon_{\text{ext}}\exp\left[-\kappa^*_{\text{ext}}(r-R)\right]/(r/R) && |\mathbf{r}|\geq R.\end{aligned} \tag{32}$$

Γ^*_{ex} for the adsorption of a supercritical HCAY fluid onto the spherical colloid particle is presented for various bulk phase and external field parameter combinations in Figs. 9, 10, 11, 12, 13, 14, 15 and 16, the chosen potential range parameter k^* is respectively 1.8, 3, and 4. For these values of the potential range parameter, critical temperatures and critical densities calculated by the uniform 5th-order TPT are respectively 1.235 and 0.31, 0.74 and 0.39, and 0.59 and 0.3954.

Figures 9–16 clearly indicates that when the coexistence bulk states are near the critical point, Γ^*_{ex} reaches a minimum: a large negative value. We call the negative maximum value of Γ^*_{ex} as 'critical depletion adsorption'. Before discussing Figs. 9–16 individually, we first propose a mechanism which helps to explain physically the critical depletion adsorption around the critical point and its relationship with the external potential parameters and bulk parameters.

Interparticle hard core repulsion induces accumulation of the fluid particles adjacent to the hard solid surface since

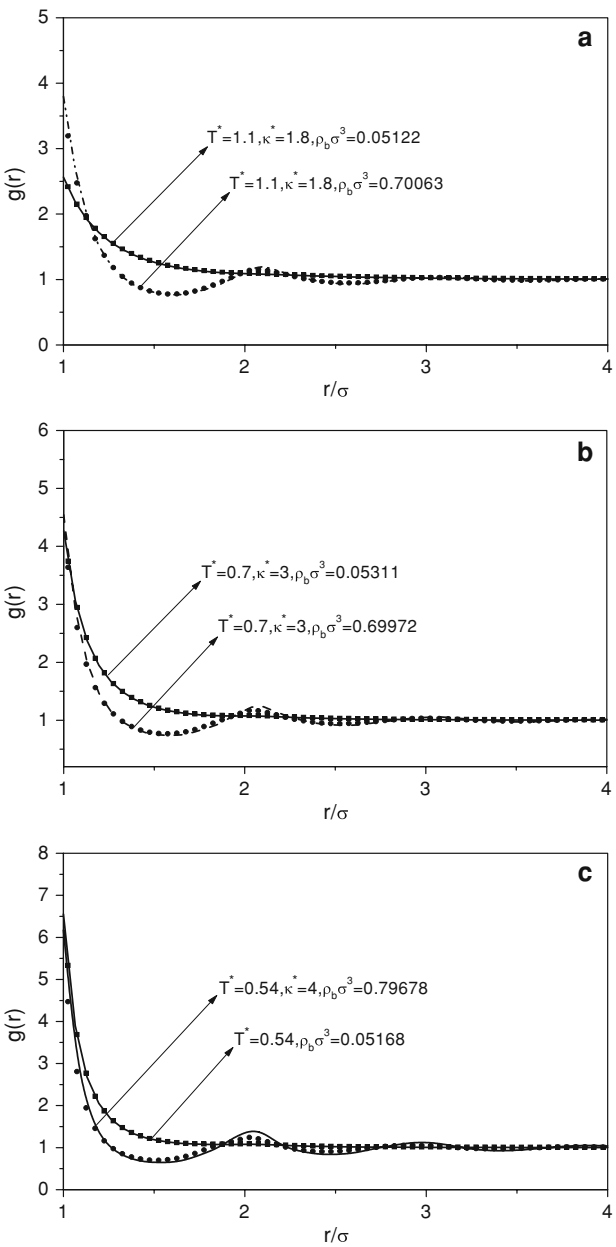

Fig. 4 **a** The RDF for the HCAY model fluid at the subcritical temperature for the bulk parameters as shown. The coexistence bulk density is either at monophasic gaseous state or at monophasic liquid state, respectively. The *lines* are for the present theoretical calculation and the *symbols* are for the simulation results [13]. **b** Same as in **a** but for the bulk parameters as shown. **c** Same as in **a** but for the bulk parameters as shown

the fluid particle can avoid to the full extent the repulsive core interaction which can be experienced to the full extent in the bulk phase when they move adjacent to the solid surface. On the contrary, the interparticle attractive tail will help to induce a depletion adsorption near the hard solid surface since the fluid particle can enjoy the attractive interaction to the full extent in the bulk phase. It is also known that the accumulation adjacent to the solid surface

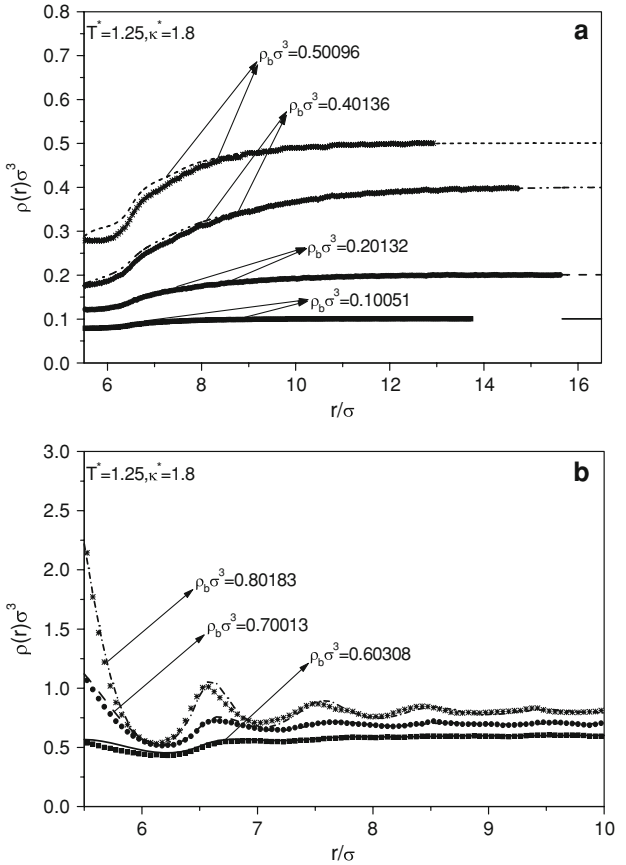

Fig. 5 **a** The theoretical (*lines*) and simulation (*symbols*) [13] results for the density profiles of the HCAY fluid at a large spherical particle of radius $R = 5.5\sigma$ at the supercritical temperatures for the shown potential range parameter and the coexistence bulk densities. **b** Same as in **a** but for the bulk coexistence densities as shown

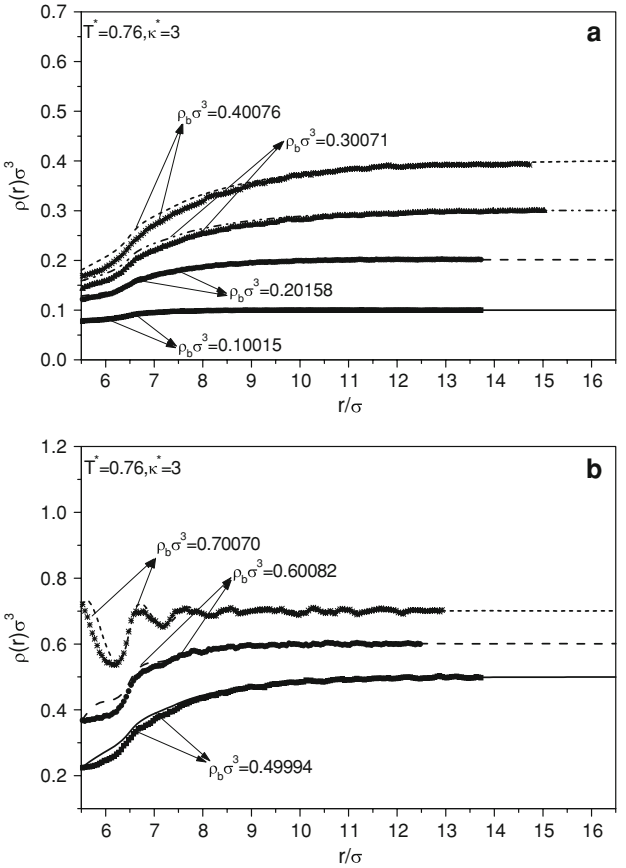

Fig. 6 **a** Same as Fig. 5a but for the bulk parameters as shown. **b** Same as in **a** but for the bulk coexistence densities as shown

can be strengthened by a high coexistence bulk density, but the depletion adsorption near solid surface induced by the interparticle attractive tail can be strengthened by a low density due to the fact that when the bulk density is high enough the repulsion interaction in the bulk phase will play more and more important role which makes the bulk environment unfavorable and the surface environment favorable. However, for the interparticle attractive tail-induced depletion, the influencing factors include additionally the critical density fluctuations. Around the critical point, the correlation length unusually rises, whole potential energy of the system is reduced due to the strong critical density fluctuations which enables the fluid particles also interact with long-range particles. When the confining geometrical size is smaller than the correlation length, to enjoy to the full extent the attraction interaction between the particles, the fluid particles will move away from the external field particle to be situated in the bulk. Therefore, the critical density fluctuations will strengthen the depletion adsorption phenomena. Obviously the influence of the critical density fluctuations on depletion adsorption will be strengthened by a highly confining geometry. For case of the hard spherical external potential, a larger radius will strengthen the critical depletion adsorption than a smaller radius does.

Figures 9, 10, 11, 12 surely display the critical depletion adsorption around the critical region of the bulk phase diagram, but how to explain why the minimum Γ^*_{ex} occurs at a coexistence bulk density larger than the respective critical density? This phenomena can also be observed in Figs. 13, 14, 15, 16. A reasonable explanation is that the long-ranged density fluctuations also exist obviously in a large region in the neighborhood of the critical point, and the intensity of such density fluctuations increases as the density increases. Therefore, for two points on an isothermal line with equal absolute distance from the critical point, the density fluctuations are stronger at the higher density point than those at the lower density point only if the two point are not far away from the critical point. Although only at the critical point the correlation length tends to infinity, the actual intensity of the density fluctuations at the critical point is not the largest, it is at some state point on the isothermal line with density higher than the critical density that the maximum intensity of the

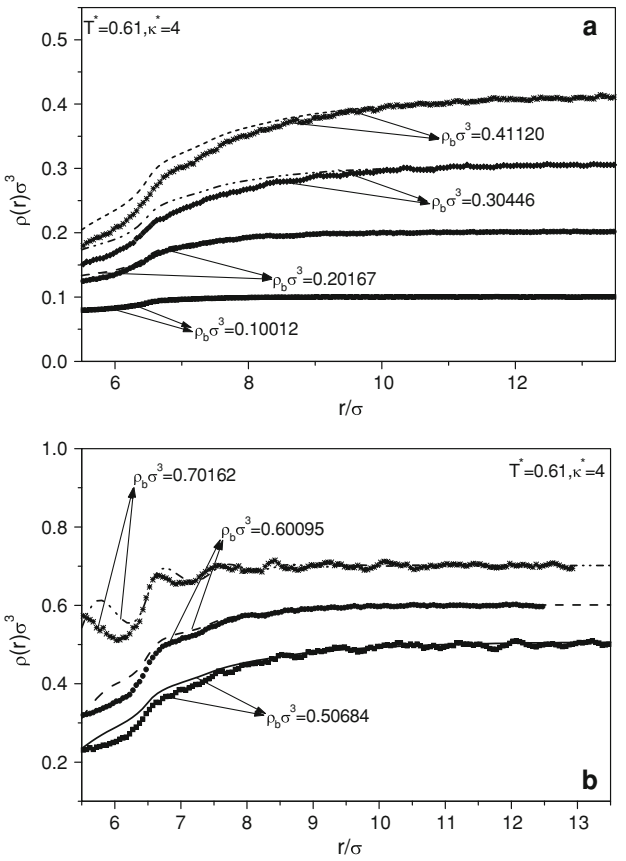

Fig. 7 **a** Same as Fig. 5a but for the bulk parameters as shown. **b** Same as in **a** but for the bulk coexistence densities as shown

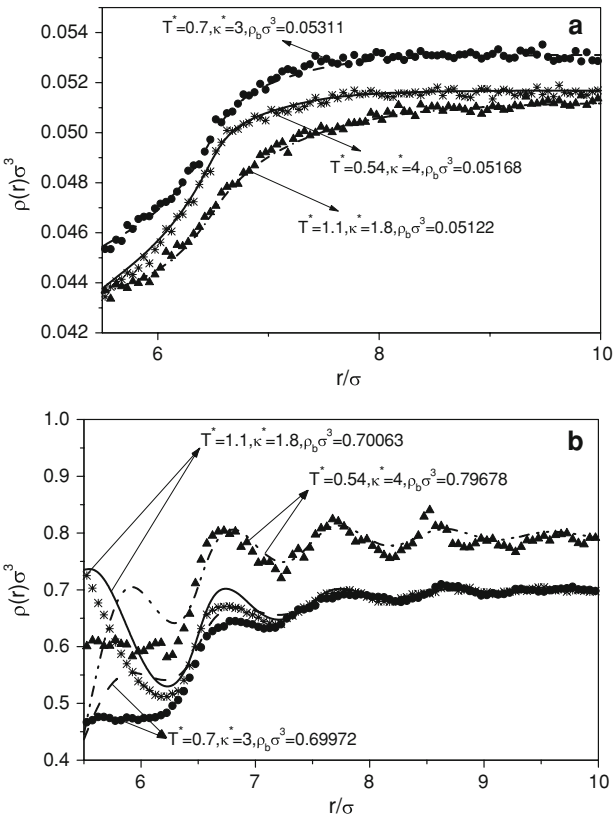

Fig. 8 **a** The theoretical (*lines*) and simulation (*symbols*) [13] results for the density profiles of the HCAY fluid at a large spherical particle of radius $R = 5.5\sigma$ at the subcritical temperature for each potential range parameter. The bulk coexistence densities are at monophasic gaseous states. **b** Same as in **a** but the bulk coexistence densities are at monophasic liquid states

density fluctuations exists. Therefore, the minimum Γ^*_{ex} occurs at a coexistence bulk density larger than the respective critical density (see Fig. 9). Figure 10 describes influence of the radius of the colloid particle on the adsorption behavior. Considering that there is a R^2 factor appearing in the denominator of Eq. 31, it can be thought that the Fig. 10 actually discloses that the depletion adsorption associated with the larger colloid particle is more obvious than that involved with the smaller colloid particle even if $R = 6\sigma$ curve is situated at the highest position and $R = 2\sigma$ curve at the lowest position. This obviously originates from the fact that the larger colloid particle constitutes a more confining restriction on the fluid particles than the smaller colloid particle, and hence the long-ranged interparticle correlation is easily truncated when the small size colloid particle is replaced by the large size colloid particle.

Figure 11 describes influence of the external potential intensity parameter $\beta\varepsilon_{ext}$ on the adsorption behavior, it is clearly observed and easily understood that the excess adsorption increases as $\beta\varepsilon_{ext}$ becomes more and more negative. The only observation worthwhile a little

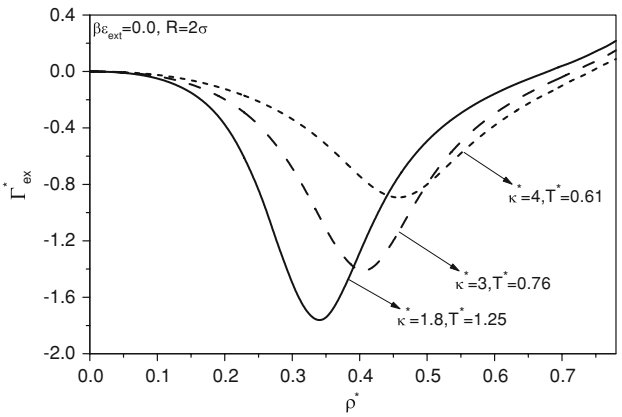

Fig. 9 The excess adsorption Γ^*_{ex} as a function of the coexistence bulk density ρ^* for three different bulk parameter combinations. The external potential is due to a neutral colloidal particle of radius $R = 2\sigma$

discussion is that along the isothermal line a maximum appears at some state point with density lower than the critical density for case of the intensity parameter of strong attraction. A feasible explanation is that the strong

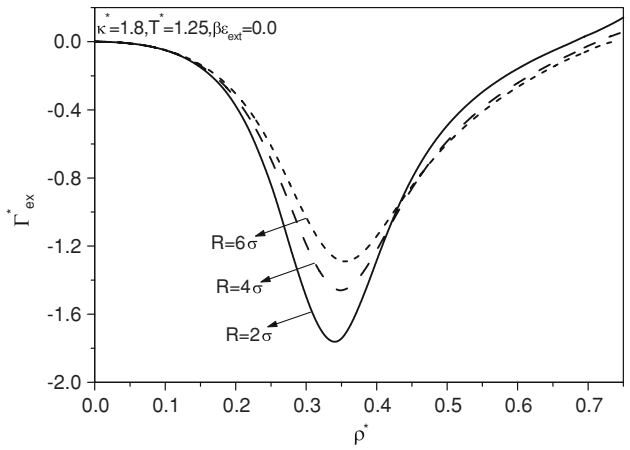

Fig. 10 The same as Fig. 9 except for only one bulk parameter combination of $k^* = 1.8$, $T^* = 1.25$ and three different neutral colloidal particle of radius $R = 2\sigma$, 4σ, 6σ, respectively as the external field

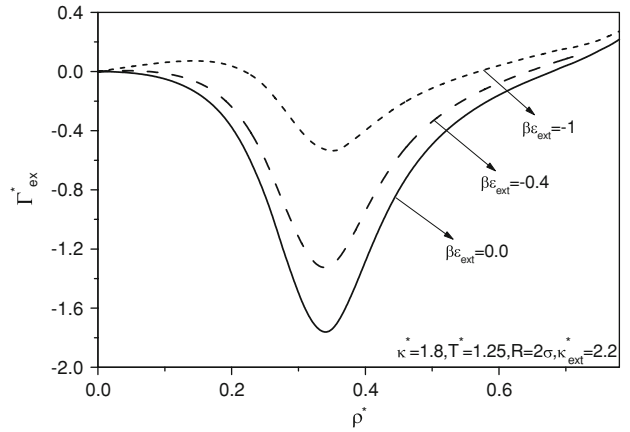

Fig. 11 The excess adsorption Γ^*_{ex} as a function of the coexistence bulk density ρ^* for three different external potential intensity parameter $\beta\varepsilon_{ext} = 0$, -0.4, -1, respectively and one external potential range parameter $\kappa^*_{ext} = 2.2$. The colloidal particle radius $R = 2\sigma$, and the bulk parameter combination is $k^* = 1.8$, $T^* = 1.25$

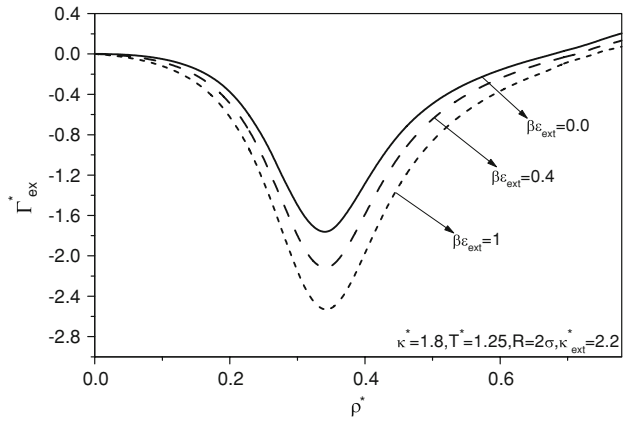

Fig. 12 The same as Fig. 11 except for three different external potential intensity parameter $\beta\varepsilon_{ext} = 0$, 0.4, 1, respectively

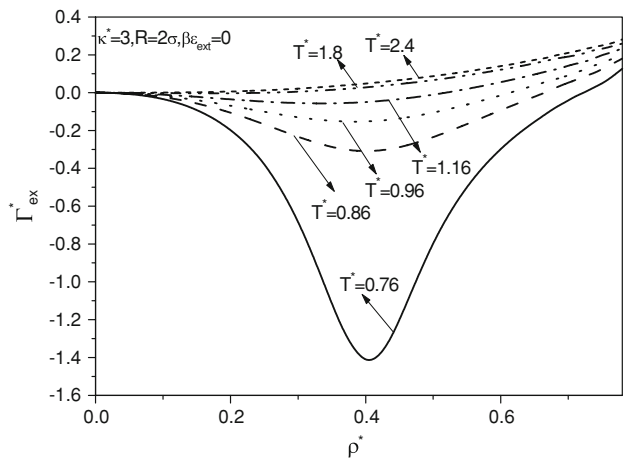

Fig. 13 The excess adsorption Γ^*_{ex} as a function of the coexistence bulk density ρ^* for six different temperature values of $T^* = 0.76$, 0.86, 0.96, 1.16, 1.8, 2.4, respectively and one potential range parameter $k^* = 3$. The external potential is due to a neutral colloidal particle of radius $R = 2\sigma$

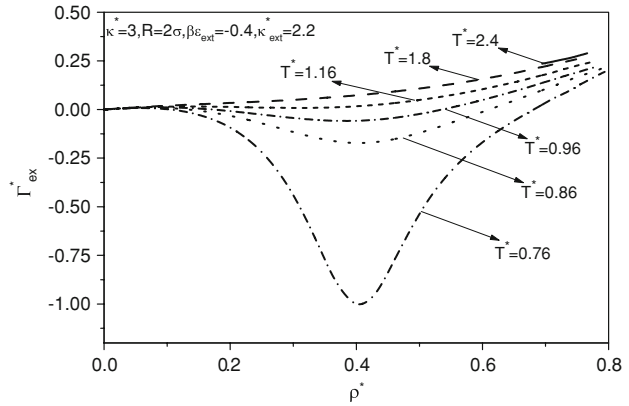

Fig. 14 The same as Fig. 13 except that the external potential is specified by $R = 2\sigma$, $\beta\varepsilon_{ext} = -0.4$ and $\kappa^*_{ext} = 2.2$

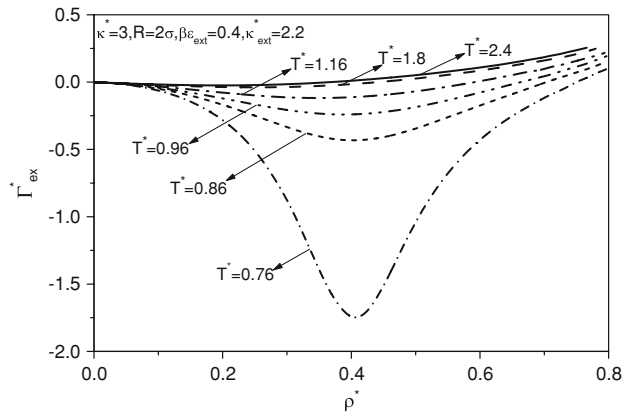

Fig. 15 The same as Fig. 13 except that the external potential is specified by $R = 2\sigma$, $\beta\varepsilon_{ext} = 0.4$ and $\kappa^*_{ext} = 2.2$

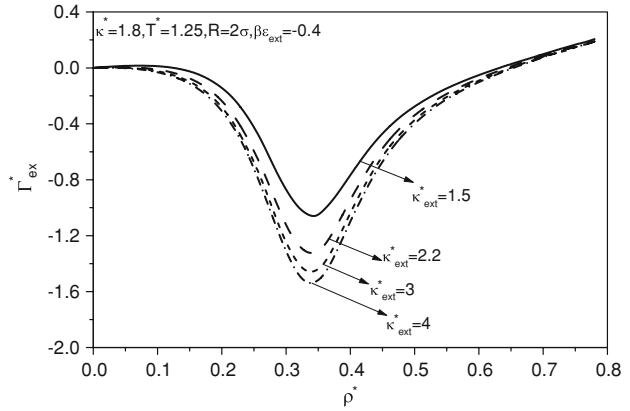

Fig. 16 The excess adsorption Γ^* as a function of the coexistence bulk density ρ^* for four different external potential range parameter of $\kappa^*_{\text{ext}} = 1.5, 2.2, 3, 4$, respectively. The bulk parameters are $k^* = 1.8$ and $T^* = 1.25$. The external field colloidal radius is $R = 2\sigma$, and the external potential intensity parameter is $\beta\varepsilon_{\text{ext}} = -0.4$

attraction external potential can counteract to a great extent the depletion effect of the surviving long-ranged density fluctuations kept for a subcritical density point. When the coexistence bulk state is free of the long-ranged density fluctuations, the regular adsorption isotherm, i.e., Γ^*_{ex} increases as the coexistence bulk density increases, is recovered. However, the regular adsorption isotherm only appears when the coexistence bulk density point is situated sufficiently away from the critical point. As the subcritical density point becomes more and more adjacent to the critical point, the regular adsorption isotherm gives place to the depletion adsorption isotherm.

On the contrary, when the attractive external potential is substituted by a repulsive one as shown in Fig. 12, the depletion effect due to the surviving long-ranged density fluctuations is strengthened by the repulsive external potential. Hence, the maximum is absent from the subcritical adsorption isotherm. Instead, the adsorption isotherm is situated at a lower position compared to that of the neutral external potential counterpart as shown in Fig. 12. Intuitively, the more repulsive the external potential is, the more negative the Γ^*_{ex} is, also in agreement with Fig. 12.

Each of the Figs. 13, 14, 15 presents a comparison of several adsorption isotherms with different temperatures, these three figures are distinguished only by different external potential intensity parameter $\beta\varepsilon_{\text{ext}}$. Two common observations can be drawn from these three figures. One is that the critical depletion adsorption happens over a wide range of the temperature, not limited only to the very neighborhood of the critical point. For neutral external potential, the limit temperature beyond which the critical depletion adsorption disappears is about $T^* = 1.4$; For attractive external potential, the limit temperature is a little lower than its neutral external potential counterpart, but still is at about $T^* = 1.2$ far higher than the critical temperature $T^*_c = 0.74$; while for repulsive external potential, the limit temperature is high up to about $T^* = 1.8$. As for the physical cause for the dependence of the limit temperature on the external potential intensity, one can explain that the repulsive external potential enables the depletion adsorption still observable even if the surviving long-ranged density fluctuations are very weak due to a sufficient distance from the critical temperature by strengthening the critical depletion adsorption. On the contrary, the attractive external potential results in opposite effect by counteracting the depletion effect of the surviving long-ranged density fluctuations.

The other general point which can be concluded from the Figs. 13–15 is that the minimum Γ^*_{ex} coexistence bulk density almost remains unchanged when the temperature changes but not far away from the critical temperature. However, when the temperature is sufficiently far away from the critical temperature, the minimum Γ^*_{ex} coexistence bulk density moves to a lower value. Such phenomena may originate from the fact that when the temperature is sufficiently high, and therefore the surviving long-ranged density fluctuations are surely weak and the critical depletion adsorption becomes sufficiently insignificant, a small increase of the coexistence bulk density can counteract the small depletion effect due to the weak surviving long-ranged density fluctuations. One only has to adjust the coexistence density to a lower value in order to make the small depletion effect still observable.

Influence of the external potential range parameter κ^*_{ext} on the adsorption isotherm is displayed in Fig. 16 which clearly shows that the longer the external potential range is, the more insignificant the critical depletion adsorption is. This is obviously due to the counteracting effect of the attractive external potential whose influence becomes more striking as the potential range becomes longer. No subcritical density maximum appears for this parameters combination, obviously this is because the attractive external potential is not sufficiently strong. One can imagine that the subcritical density inducing the maximum Γ^*_{ex} will appear if one adjusts κ^*_{ext} to a smaller value or $\beta\varepsilon_{\text{ext}}$ to a more negative value or a combination of the two adjustments.

Figure 17a and b describe subcritical adsorption behavior respectively for low density vapor side and high density liquid side as the coexistence bulk phases. For the neutral colloid particle, it clearly is found that the excess adsorption Γ^*_{ex} shows a decreasing tendency as the vapor-liquid coexistence densities are approached respectively from low density vapor side or from high density liquid side, the observation fully indicates that the long-ranged critical density fluctuations still survive in the neighborhood of subcritical vapor-liquid coexistence curve.

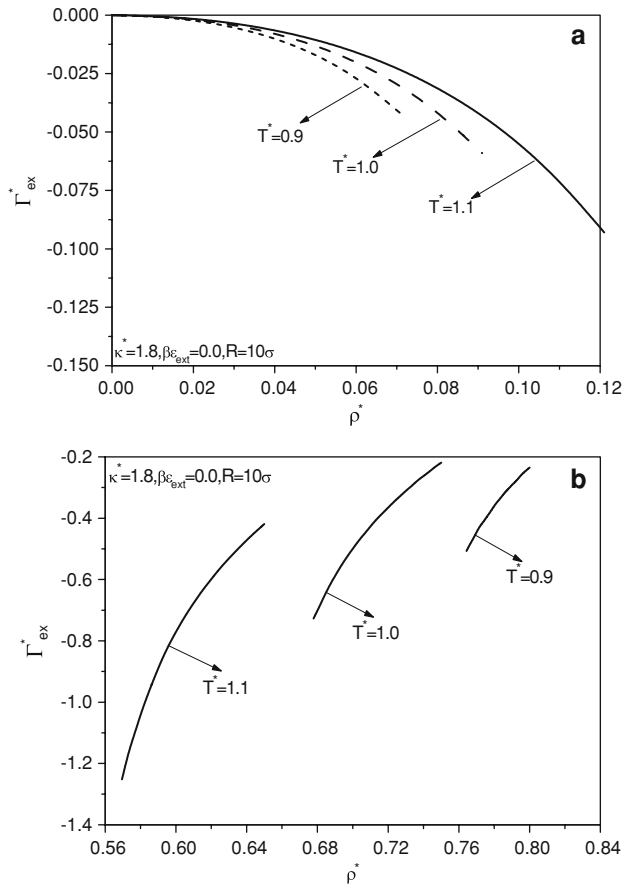

Fig. 17 **a** The excess adsorption Γ^*_{ex} as a function of the coexistence bulk density ρ^* for three different subcritical temperature of $T^* = 0.9$, 1, 1.1, respectively. The coexistence bulk densities are respectively adjacent to respective bulk vapor-liquid coexistence gaseous densities. The potential range parameter is $k^* = 1.8$,, and the external field is due to a neutral colloidal particle of radius $R = 10\sigma$. **b** Same as in **a** but the coexistence bulk densities are adjacent to respective bulk vapor–liquid coexistence liquidous densities

Figure 17a and b also discloses a pattern which declares that the excess adsorption Γ^*_{ex} corresponding to the bulk vapor–liquid coexistence densities decreases as the temperature increases. This observation fully indicates that with the dropping of the temperature the depletion adsorption is weakened. Therefore, one can conclude that the critical density fluctuations become weakened as the fluid is situated away from the critical temperature, but the surviving critical density fluctuations in the neighborhood of subcritical vapor–liquid coexistence curve still can show up more or less.

Figures 18 and 19 describe the adsorption isochores for different subcritical and supercritical densities. One clearly observes that as the dropping of the temperature and the approaching of the coexistence bulk density to the bulk vapor–liquid coexistence densities the excess adsorption Γ^*_{ex} shows a quickly decreasing tendency. Particularly, for the same temperature the most negative Γ^*_{ex} corresponds to the isochore whose coexistence bulk density is the most adjacent to the critical density. This also indicates that the more adjacent to the critical point, the more intensive the critical density fluctuations are.

Figure 20 describes the adsorption of the HCAY particles onto a colloidal particle which interacts with the HCAY particles by an attractive tail besides the hard repulsion, the two subfigures are distinguished only by different external potential parameters combinations, vertical lines indicate the coexistence densities. To avoid omitting of possible first-order pre-wetting transition which generally happens for single wall external potential also with an attractive tail, the coexistence bulk density calculated increases until the numerical code diverges or the vapor–liquid coexistence gaseous density is overtaken. Choice of the colloidal particle radius $R = 2\sigma$ is made to more clearly detect the possible effect due to the surface curvature. Contrary to the accelerating decreasing of the excess adsorption Γ^*_{ex} as the coexistence bulk gas density approaches to the bulk vapor–liquid coexistence gaseous density for case of the neutral colloidal particle (see Figs. 17a, 18), the present Γ^*_{ex} shows an accelerating increase as the bulk vapor–liquid coexistence gaseous density is approached. This completely dissimilar behavior obviously originates from a coupling between the attractive tail of the external potential imposed on the HCAY particle and the interparticle attractive Yukawa tail, such coupling is significantly strengthened by the long-ranged density fluctuations retained in the region of the phase diagram very adjacent to the bulk vapor–liquid coexistence curve. As we use the calculated density profile in situation of preceding smaller coexistence bulk density as input for the situation of larger coexistence bulk density, a numerical instability of our code will mark a diverging adsorption. If the numerical instability does not appear at all even if the vapor–liquid coexistence gaseous density is overtaken, one can conclude that no wetting transition occurs for the parameter combination under consideration. For case of the diverging adsorption, even if one employs very different density profile as input, the final adsorption isotherms take the same appearances, this fully indicates that what occurs is a round wetting transition instead of a first-order pre-wetting transition [40] whose occurrence associated with the single wall external potential is confirmed numerously. Furthermore, occurrence of the round wetting transition deeply depends on a total attractive intensity of the external field. The attractive intensity obviously depends on both external potential range parameter κ^*_{ext} and external potential intensity parameter $\beta\varepsilon_{ext}$. A decreasing of κ^*_{ext} or an increasing of $\beta\varepsilon_{ext}$ or combination of the two changes will lead to a large attractive intensity which will induce round wetting transition. On the contrary, a small attractive intensity will not be associated with any kind of wetting

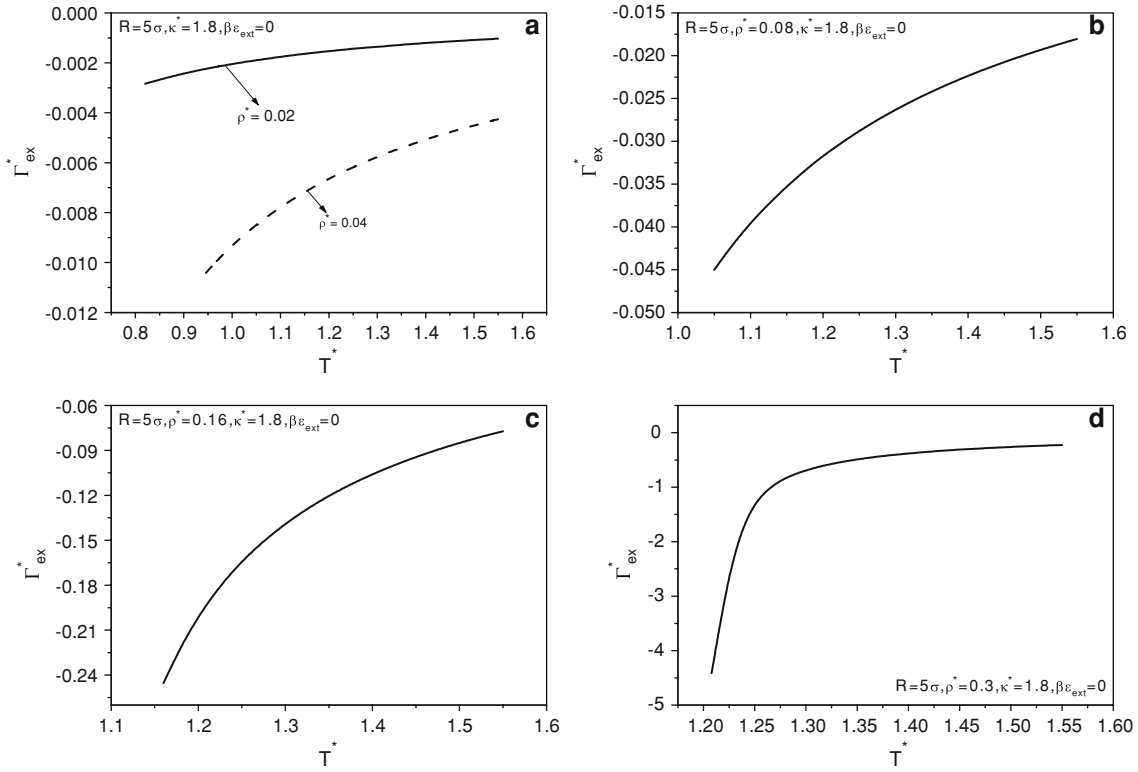

Fig. 18 **a** The excess adsorption Γ^*_{ex} as a function of temperature for subcritical coexistence bulk densities of $\rho^* = 0.02, 0.04$. The potential range parameter is $k^* = 1.8$, and the external field is due to a neutral colloidal particle of radius $R = 5\sigma$. **b** Same as in **a** but the subcritical coexistence bulk density of $\rho^* = 0.08$. **c** Same as in **a** but the subcritical coexistence bulk density of $\rho^* = 0.16$. **d** Same as in **a** but the near critical coexistence bulk density of $\rho^* = 0.3$

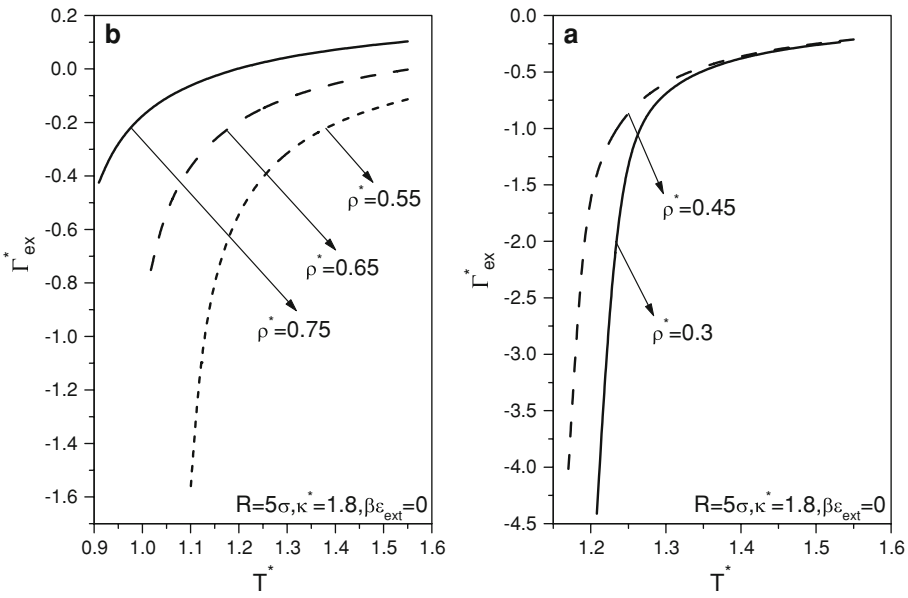

Fig. 19 **a** The same as Fig. 18a except for supercritical coexistence bulk density of $\rho^* = 0.45$ and near critical coexistence bulk density of $\rho^* = 0.3$. **b** Same as in **a** but the supercritical coexistence bulk densities of $\rho^* = 0.55$, 0.65, 0.75

transitions as shown in Fig. 20a and b. To indicate that the absence of the first-order pre-wetting transition is inherent to the spherical geometrical body, not due to the chosen sample temperature being above the pre-wetting critical point temperature, we calculate for a smaller reduced temperature of $T^* = 0.85$, the calculated results are presented in Fig. 21. To avoid omitting of possible first-order pre-wetting transition which generally happens for single wall external potential also with an attractive tail, we choose a larger radius of $R = 10\sigma$, Fig. 21 shows that not

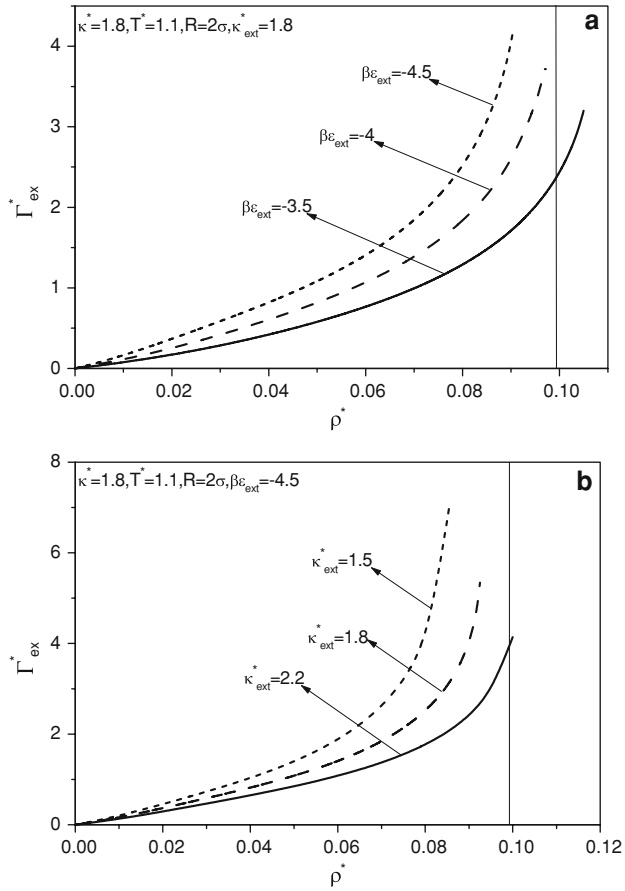

Fig. 20 **a** The excess adsorption Γ^*_{ex} as a function of the coexistence bulk density ρ^* for three different external potential intensity parameters of $\beta\varepsilon_{ext} = -3.5,\ -4,\ -4.5$, respectively. The bulk parameters are $k^* = 1.8$ and $T^* = 1.1$, and the external field colloidal particle radius is $R = 2\sigma$. The external potential range parameter is $\kappa^*_{ext} = 1.8$. **b** The excess adsorption Γ^*_{ex} as a function of the coexistence bulk density ρ^* for three different external potential range parameter of $\kappa^*_{ext} = 1.5,\ 1.8,\ 2.2$ respectively. The bulk parameters are $k^* = 1.8$ and $T^* = 1.1$, and the external field colloidal particle radius is $R = 2\sigma$. The external potential intensity parameters is $\beta\varepsilon_{ext} = -4.5$

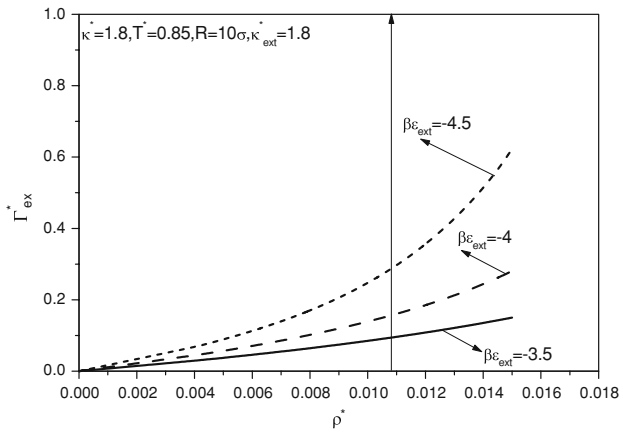

Fig. 21 The same as Fig. 20a except for different parameter combinations as shown in the figure

only the first-order pre-wetting transition is still absent, but also the round wetting transition disappears. The observation of absence of the first-order pre-wetting transition fully lends support to the conclusion that the first-order pre-wetting transition is truly not associated with the spherical geometrical body. On the other hand, disappearance of the round wetting transition in situation of sufficiently low temperature enables one to conclude that the critical density fluctuations in the neighborhood of subcritical vapor-liquid coexistence curve become more and more weakened as the state point is situated far away from the critical temperature. It should be pointed out that the first-order pre-wetting transition occurs for a wall external potential even at a temperature low down to the triple-point temperature [41]. Our observation is in agreement with a previous theoretical analysis based on a thermodynamic consideration [42] and a phenomenological Landau mean field theory [43], the theoretical analysis declares that the surface curvature suppresses the first-order pre-wetting transition and the shift of the wetting transition temperature is proportional to ln R/R for large R. Then, what remains to be answered is how to explain physically why the wetting transition temperature increases as the colloidal particle radius R decreases? Obviously the single wall is a stronger confining geometry than the single sphere is; for the type of the external potential inducing the wetting transition, the spherical geometry only exerts a weaker attractive force on the fluid particles than the wall geometry does. Hence, to induce the wetting transition which originates from the interaction between the fluid interparticle attraction and the attractive external potential strengthened by the surviving long-ranged density fluctuations, more surviving long-ranged density fluctuations are needed for the case of the spherical geometry than for the wall geometry. As pointed out above, the more adjacent to the critical temperature the coexistence bulk state is, the stronger the surviving long-ranged density fluctuations are. Therefore, the wetting transition temperature is higher for the spherical geometry than for the wall geometry.

The readers may have doubt that use of such high order perturbation theories may be relevant if it is done exactly, or at least within an extremely good level of confidence, for the perturbation scheme. However, what is used here is a SWDA [21] borrowed from the hard-sphere fluid. Any possible gain in the quality of the results from 3rd- to 5th-order perturbation is overwhelmed by the low quality of the approximation used to evaluate the perturbation contributions.

To answer whether there is a sign of any significant improvement due to the extension from 3rd- to 5th-order perturbation scheme, we employ the present non-uniform

TPT-ZDL-PTS formalism for calculation of the density profiles of a hard sphere plus square well (SW) fluid confined within a hard spherical cavity as simulated in Ref. [6]. The hard sphere plus square well potential is given by

$$\begin{aligned} u(r) &= \infty, \quad r < \sigma \\ &= -\varepsilon, \quad \sigma < r < \lambda\sigma, \end{aligned} \tag{33}$$

the external potential due to the hard spherical cavity is given by

$$\begin{aligned} \varphi_{\text{ext}}(\mathbf{r}) &= \propto \quad |\mathbf{r}| > R - 0.5\sigma \\ &= 0 \quad |\mathbf{r}| < R - 0.5\sigma. \end{aligned} \tag{34}$$

The reduced well width under consideration is $\lambda = 1.5$, the coexistence bulk phases are respectively $T^* = 1.228$, $\rho_b\sigma^3 = 0.31895$ for state 1, and $T^* = 1.25372$, $\rho_b\sigma^3 = 0.31973$ for state 2.

Figure 22a presents $f_{\text{ex-tail}}$ (ρ_b) as a function of the bulk density $\rho_b\sigma^3$ for the two chosen temperatures respectively from the uniform 3rd- and 5th-order TPT. Figure 22b presents the theoretical results respectively from the non-uniform 5th-order TPT-ZDL-PTS and the non-uniform 3rd-order TPT-ZDL-PTS together with the corresponding simulation data from Ref. [6]. Figure 22b clearly displays a significant improvement due to the extension from 3rd- to 5th-order perturbation scheme. Hence one does not feel concerned about the possibility that the approximation used to evaluate the perturbation contributions overwhelms the gain in the quality of the results from 3rd- to 5th-order perturbation as input, the present non-uniform TPT-ZDL-PTS formalism accurately and faithfully reflects any possible minor gain in accuracy of the input in the final results.

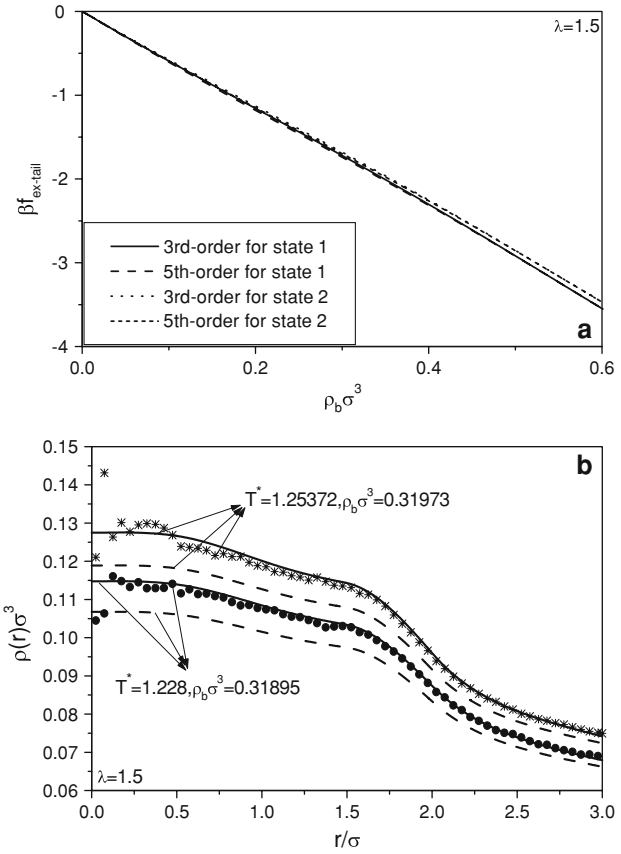

Fig. 22 **a** The $f_{\text{ex-tail}}$ (ρ_b) as a function of the bulk density $\rho_b\sigma^3$ for two states of the hard sphere plus SW fluid respectively from the uniform 3rd and 5th-order TPT. **b** Density profile of the hard sphere plus SW fluid in the hard spherical cavity of radius $R = 3.5\sigma$ in coexistence with the bulk fluid near the critical point. *Symbols* are for the GCEMC simulation results [6], while *solid lines* are for the present non-uniform 5th-order TPT-ZDL-PTS, *dashed lines* are for the non-uniform 3rd-order TPT-ZDL-PTS

4 Summary

The present paper extended the uniform TPT to its non-uniform counterpart, the resultant non-uniform 5th-order TPT-ZDL-PTS is implemented in the framework of the classical DFT, and is free from numerical solution of the OZ integral equation, therefore is applicable to both the subcritical and supercritical temperature regions. The accuracy of the non-uniform 5th-order TPT-ZDL-PTS for the density profiles of the HCAY fluid confined by various geometries is generally higher than the 3rd + 2nd-order perturbation DFT [12, 13]. Considering that the non-uniform 5th-order TPT-ZDL-PTS is based on several ansatzs for the bulk 2nd-order DCF, therefore its reliability for other model potentials, particularly for those effective potentials which are of complicated mathematical forms, is worthwhile further separate investigation. Comprehensive investigation about the adsorption of the HCAY fluid under influence of external field around the critical point and adjacent to the vapor–liquid coexistence curve is carried out, we find the interesting critical depletion adsorption phenomena which can be explained by the long-ranged critical density fluctuations being marked in these regions of the phase diagram.

Another finding is that the critical density fluctuations actually exist in a wide region of the diagram. For the supercritical state, only if the temperature is higher than the critical temperature by 60–140% do the critical density fluctuations become trivial. Of course, the particular percentage depends on the external potential parameters such as the external potential range parameter κ^*_{ext}, the external potential intensity parameter $\beta\varepsilon_{\text{ext}}$, and the colloid particle radius, etc. For the subcritical state, the surviving critical density fluctuations will still play role in influencing the adsorption even if the temperature is lowered to far below the critical temperature. One can expect that the limit temperature beyond which the surviving critical density

fluctuations do not influence significantly on the adsorption behavior, depends on the external potential parameters.

In the end, the wetting transition around a colloidal particle is investigated. The present microscopic theoretical calculation tests and verifies a previous conclusion drawn from a thermodynamic analysis [42] and a phenomenological Landau mean field theory calculation [43] that the surface curvature suppresses the first-order pre-wetting transition and one should observe rounded transition, and the wetting transition temperature shifts to a higher value by the surface curvature.

It should be pointed out that the critical depletion adsorption will influence the effective potentials [44–51] between the colloidal particles immersed in a small size solvent bath, and certainly will also influence the phase behavior [52–59] of complex fluids. All of these topics and more detailed research for the wetting transitions in confined conditions by the present non-uniform 5th-order TPT-ZDL-PTS will be investigated in future publications.

Acknowledgments This project is supported by the National Natural Science Foundation of China (Grant No. 20673150).

References

1. Adib AB (2007) Phys Rev E 75:061204, and references therein
2. Zhou S (2007) J Chem Phys 127:084512, and references therein
3. Lu M, Bevan MA, Ford DM (2007) J Chem Phys 127:164709, and references therein
4. Punnathanam S, Corti DS (2007) Phys Rev E 69:036105
5. Siderius DW, Corti DS (2007) Phys Rev E 75:011108
6. Zhou S (2006) Phys Rev E 74:031119
7. Zhou S (2006) J Chem Phys 125:144518
8. Zhou S (2007) J Phys Chem B 111:10736
9. Zwanzig RW (1954) J Chem Phys 22:1420
10. Barker JA, Henderson D (1976) Rev Mod Phys 48:587
11. Barker JA, Henderson D (1967) J Chem Phys 47:2856
12. Zhou S (2003) Commun Theor Phys (Beijing, China) 40:721
13. Zhou S, Jamnik A (2005) J Chem Phys 122:064503
14. Carnhan NF, Starling KE (1969) J Chem Phys 51:635
15. Henderson D (1992) Fundamentals of inhomogeneous fluids. Marcel Dekker, New York
16. Nordholm S, Johnson M, Freasier BC (1980) Aust J Chem 33:2139
17. Johnson M, Nordholm S (1981) J Chem Phys 75:1953
18. Tarazona P (1985) Phys Rev A 31:2672
19. Curtin WA, Ashcroft NW (1985) Phys Rev A 32:2909
20. Rosenfeld Y (1989) Phys Rev Lett 63:980
21. Zhou S (1999) J Chem Phys 110:2140
22. Greberg H, Paolini GV, Satherley J, Penfold R, Nordholm S (2001) J. Colloid Interface Sci 235:334
23. Patra CN (1999) J Chem Phys 111:9832
24. Kim SC, Suh SH, Lee CH, Lee H (1999) J Korean Phys Soc 35:350
25. Patra CN (1999) J Chem Phys 111:6573
26. Zhou S (2001) Phys Rev E 63:061206
27. Zhou S (2002) New J Phys 4:36
28. Götze IO, Archer AJ, Likos CN (2006) J Chem Phys 124:084901, and reference therein
29. Tang Z, Scriven LE, Davis HT (1991) J Chem Phys 95:2659
30. Kol A, Laird BB (1997) Mol Phys 90:951
31. Sweatman MB (2001) Phys Rev E 63:031102
32. Kim S-C, Lee SH (2004) J Phys Condens Matter 16:6365
33. Thiele E (1963) J Chem Phys 39:474
34. Wertheim MS (1963) Phys Rev Lett 19:321
35. Zhou S (2003) Phys Lett A 319:279
36. Henderson JR (1991) In: Henderson D (ed) Fundamentals of inhomogeneous fluids. Marcel Dekker, New York, p 23
37. Zhou S (2006) J Colloid Interface Sci 298:31
38. Percus JK (1964) In: Frisch HL, Lebowitz AL (eds) The equilibrium theory of classical fluids. Benjamin, New York, p 113
39. Zhou S, Jamnik A (2006) Phys Rev E 73:011202
40. Ancilotto F, Toigo F (2000) J Chem Phys 112:4768
41. Sukhatme KG, Rutledge JE, Taborek P (1998) Phys Rev Lett 80:129
42. Holyst R, Poniewierski A (1987) Phys Rev B 36:5628
43. Marconi UMB (1988) Phys Rev A 38:6267
44. Mognetti BM, Oettel M, Yelash L, Virnau P, Paul W, Binder K (2008) Phys Rev E 77:041506
45. Kim S-C, Suh S-H, Seong B-S (2007) J Chem Phys 127:114903
46. Chakrabarti J, Chakrabarti S, Löwen H (2006) J Phys Condens Matter 18:L81
47. Abbas S, Lodge TP (2007) Phys Rev Lett 99:137802
48. Qin Y, Fichthorn KA (2007) J Chem Phys 127:144911
49. Dahirel V, Jardat M, Dufrêche J-F, Turq P (2007) J Chem Phys 127:095101
50. Domínguez A, Oettel M, Dietrich S (2007) J Chem Phys 127:204706
51. Dominguez A, Frydel D, Oettel M (2008) Phys Rev E 77:020401
52. Lomba E, Almarza NG, Martín C, McBride C (2007) J Chem Phys 126:244510
53. Lee J, Popov YO, Fredrickson GH (2008) J Chem Phys 128:224908
54. Orea P (2005) J Chem Phys 123:144704
55. Orea P (2009) J Chem Phys 130:104703
56. Liétor-Santos JJ, Chávez-Páez M, Márquez M, Fernández-Nieves A, Medina-Noyola M (2007) Phys Rev E 76:050403
57. Ramiro-Manzano F, Bonet E, Rodriguez I, Meseguer F (2007) Phys Rev E 76:050401
58. Merabia S, Pagonabarraga I (2007) J Chem Phys 127:054903
59. Cappallo N, Lapointe C, Reich DH, Leheny RL (2007) Phys Rev E 76:031505